JACS
JOURNAL OF THE AMERICAN CHEMICAL SOCIETY
Article
pubs.acs.org/JACS

A Generalized Electrochemical Aggregative Growth Mechanism

Jon Ustarroz,[†] Joshua A. Hammons,[†] Thomas Altantzis,[‡] Annick Hubin,[†] Sara Bals,[‡] and Herman Terryn*,[†]

[†]Research Group Electrochemical and Surface Engineering (SURF), Vrije Universiteit Brussel, Pleinlaan 2, 1050 Brussels, Belgium
[‡]EMAT, University of Antwerp, University of Antwerp, Groenenborgerlaan 171, 2020 Antwerp, Belgium

Supporting Information

ABSTRACT: The early stages of nanocrystal nucleation and growth are still an active field of research and remain unrevealed. In this work, by the combination of aberration-corrected transmission electron microscopy (TEM) and electrochemical characterization of the electrodeposition of different metals, we provide a complete reformulation of the Volmer−Weber 3D island growth mechanism, which has always been accepted to explain the early stages of metal electrodeposition and thin-film growth on low-energy substrates. We have developed a Generalized Electrochemical Aggregative Growth Mechanism which mimics the atomistic processes during the early stages of thin-film growth, by incorporating nanoclusters as building blocks. We discuss the influence of new processes such as nanocluster self-limiting growth, surface diffusion, aggregation, and coalescence on the growth mechanism and morphology of the resulting nanostructures. Self-limiting growth mechanisms hinder nanocluster growth and favor coalescence driven growth. The size of the primary nanoclusters is independent of the applied potential and deposition time. The balance between nucleation, nanocluster surface diffusion, and coalescence depends on the material and the overpotential, and influences strongly the morphology of the deposits. A small extent of coalescence leads to ultraporous dendritic structures, large surface coverage, and small particle size. Contrarily, full recrystallization leads to larger hemispherical monocrystalline islands and smaller particle density. The mechanism we propose represents a scientific breakthrough from the fundamental point of view and indicates that achieving the right balance between nucleation, self-limiting growth, cluster surface diffusion, and coalescence is essential and opens new, exciting possibilities to build up enhanced supported nanostructures using nanoclusters as building blocks.

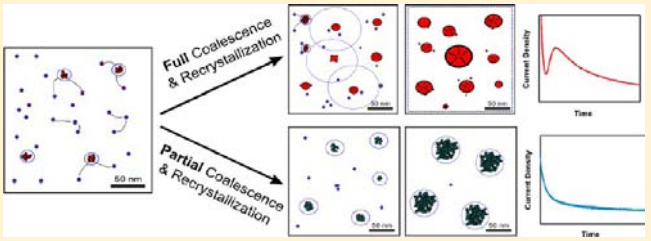

INTRODUCTION

Metal nanocrystals are of great interest due to their unique properties which differ from their bulk counterparts and can be tuned by adjusting their size and shape.[1,2] When supported on different substrates, they represent the cornerstone for numerous applications in different fields, such as catalysis[2,3] or sensing.[4,5] They can be synthesized by multiple methods, reviewed many times,[2] with colloidal synthesis and other solution based methods being the most common approach.[6,7] Nonetheless, colloids may lose some of their properties due to the organic ligands used during the synthesis procedure, or because of unwanted aggregation during deposition on a given support.[8] In contrast, electrochemical deposition allows the growth of the nanostructures in one step, directly on the final support, improving the electron pathway within the substrate, nanostructure, and environment. Consequently, the technique has been proven effective to obtain highly electroactive nanostructures with potential for fuel cell[9,10] or (bio)sensing[4] applications.

One of the key issues to benefit from the fascinating properties of nanostructures is to understand their formation mechanisms in order to achieve a good control of their morphological and structural parameters. However, despite the increasing number of publications in the field, the early stages of nanocrystal formation are still under discussion. Nucleation and growth phenomena have been thoroughly studied for more than a century for colloidal syntheses,[11] thin film growth,[12] and electrochemical deposition processes,[13] among others. This has resulted in a classic nucleation and growth theory which predicts that nanocrystals grow irreversibly by atomic addition until the reaction is halted. In colloidal synthesis, nanoparticle growth has been traditionally described by burst nucleation and slow growth, introduced by LaMer,[14] and slow nucleation and fast autocatalytic-growth, developed by Watzky, Finke, and co-workers.[15] Both mechanisms differ in many aspects but they are based on the concept that nanocrystal growth only proceeds by direct atomic attachment. Nonetheless, aberration-corrected atomic resolution transmission electron microscopy (TEM) has recently become accessible for colloid chemists to shed light on nanocrystal growth mechanisms.[16] In addition, the development of technologies for in situ characterization has made it possible to study the nucleation and growth of nanoparticles by in situ TEM[17−19] and Small Angle X-ray Scattering

Received: March 13, 2013
Published: June 28, 2013

dx.doi.org/10.1021/ja402598k | J. Am. Chem. Soc. 2013, 135, 11550−11561

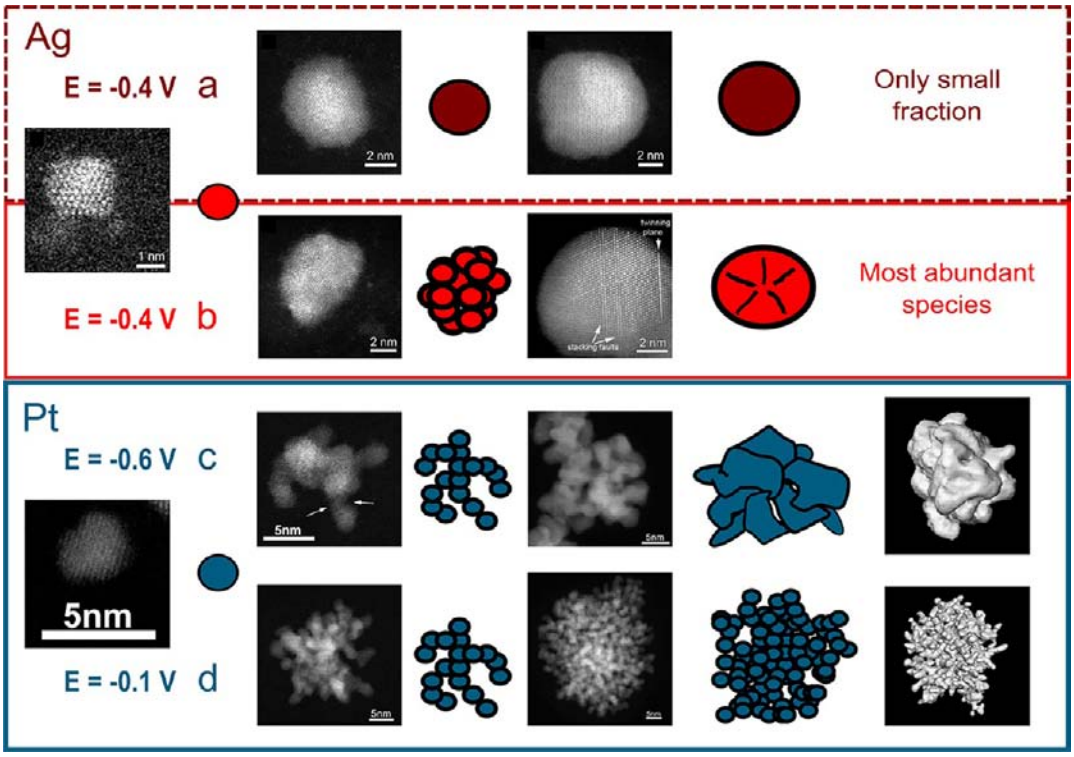

Figure 1. Schematic diagram showing the growth pathways observed by HAADF-STEM observation during the electrodeposition of silver (a,b) and platinum (c,d) onto CCTGs. (a) Growth by direct attachment resulting in defect-free monocrystalline nanoparticles. (b) Growth by nanocluster aggregation and full coalescence resulting in monocrystalline nanoparticles with defects. (c) Growth by nanocluster aggregation and partial coalescence resulting into porous nanostructures. (d) Growth by nanocluster aggregation and small extent of coalescence resulting in ultraporous dendritic nanostructures.

(SAXS)[20−22] indicating that small nanoparticles grow by aggregation and coalescence to a bigger extent than by monomer addition. Similar growth pathways have also been observed, based on ex-situ characterization of the evolution of nanocluster size distributions.[23,24] In fact, the formation of nanostructures by oriented attachment of nanocrystal building blocks has been reviewed recently[25] and evidence for this growth pathway is being reported in the formation of other type of nanostructures such as protein−inorganic hybrid nanoflowers[26] or dendritic nanostructures.[27−29]

However, electrochemical deposition and thin film growth in general have always been studied considering atomic incorporation as the only growth mechanism. In these cases, characterization has been traditionally limited to nanometer scale characterization by surface analysis techniques such as AFM/STM or FESEM, limiting the access to atomic-scale information. On top of that, the fact that nucleation takes part on a surface has led to assumptions that nuclei stand still on the substrate and, in the case of metal deposition onto low-energy substrates, that they grow radially by direct attachment along with the well-known Volmer−Weber 3D island growth mechanism. Based on these assumptions, measurements of the current−time transients obtained by potentiostatic electrochemical deposition have been correlated with the growth of randomly distributed hemispherical nuclei allowing a nucleation rate to be extracted and hence predicting the evolution of particle number density and size with deposition time.[30] This approach has been used and reviewed on countless occasions,[31] but it has been reported in many cases that it cannot explain experimental observations appropriately,[9,32−36] which questions its validity. Still, growth by nanocluster aggregation and coalescence has never been seriously considered, although suggested by some authors to account for irregular deposit morphologies.[34,35]

Nevertheless, we recently showed that by using carbon coated TEM grids (CCTGs) as electrochemical electrodes, we gain access to atomic-scale characterization of as-electrodeposited nanostructures correlated with electrochemical measurements.[37] In this way, we proved that silver electrodeposition on carbon does not proceed by a Volmer−Weber mechanism. In contrast, ultrasmall nanoclusters of $d \approx 1-2$ nm diffuse over the carbon substrate, aggregate, and only grow by atomic addition after complete recrystallization.[33] Furthermore, by means of electron tomography, aberration-corrected HAADF-STEM, and in situ SAXS, we proved that platinum electrodeposition results into ultraporous dendritic nanostructures produced by the aggregation, self-alignment, and partial coalescence of size-monodispersed nanoclusters of $d \approx 2$ nm.[38] Consequently, we suggested that the Volmer−Weber island growth mechanism should be revised toward an Electrochemical Aggregative Growth Mechanism which includes nanocluster surface diffusion, aggregation, and coalescence as the main mechanisms of early nanocrystal growth.

This work combines aberration-corrected HAADF-STEM, FESEM and electrochemical characterization of different electrochemical deposition systems to unravel the processes underlying metal electrodeposition on low energy substrates. We elaborate therefore on a Generalized Electrochemical Aggregative Growth Mechanism which mimics the atomistic processes during the early stages of thin-film growth[39] by incorporating nanoclusters of a few nm as building blocks. We finally discuss the influence of new key parameters on the

growth mechanism, on the interpretation of potentiostatic current transients, and on the morphology of the resulting electrodeposited nanostructures. The understanding of the proposed growth mechanism allows better control of electrochemical deposition processes toward obtaining supported nanostructures with desired morphology and enhanced properties.

EXPERIMENTAL SECTION

Platinum and silver electrochemical deposition has been carried out using 1×10^{-3} M H_2PtCl_6 + 0.1 M KCl[38] and 1×10^{-3} M $AgNO_3$ + 0.1 M KNO_3,[33] respectively. In both cases, solutions have been previously deareated by N_2. Electrochemical measurements have been performed using an AUTOLAB PGSTAT 100 in a three-electrode configuration with an Ag/AgCl reference electrode and a Pt counter electrode. All the potentials mentioned throughout the paper are referred to Ag/AgCl. In order to perform TEM analysis on as-prepared samples, carbon coated TEM grids from EMS (300mesh, CF 300Au) have been used as electrochemical working electrodes. Further details are described elsewhere.[33,37,38] Ex situ morphological and structural characterization of the electrodeposited nanostructures has been performed using a JEOL JSM-7000F FESEM operated at 20 kV, a FEI Tecnai G20 electron microscope operated at 200 kV, and a double aberration-corrected FEI Titan 50−80 electron microscope operated at 300 kV.

RESULTS AND DISCUSSION

Evaluation of Different Growth Pathways. Silver and platinum nanoparticles have been grown onto CCTGs by potentiostatic electrodeposition at different potentials and deposition times. Further experimental details are provided elsewhere.[33,37,38] Figure 1 shows a summary of the different growth pathways inferred from high magnification HAADF-STEM characterization. When the main growth mechanism is atomic addition, monocrystalline defect-free nanoparticles such as of growth pathway *'a'* are expected to be the most abundant species. However, in the case of silver electrodeposition, only a very small portion of particles are found to present such a structure. Contrarily, most of the silver nanoparticles are found to grow through a mechanism such as the one depicted by growth pathway *'b'*. It can be summarized as the aggregation of randomly oriented nanoclusters of $d \approx 1-2$ nm, followed by total recrystallization and further epitaxial growth by incorporation of Ag atoms through direct attachment (reduction of Ag^+ ions on the particle surface). After this stage, nanoparticles are monocrystalline but display defects such as stacking faults or twinning planes, witnessing previous coalescence events.[33] The figures correspond to silver nanostructures obtained at $E = -0.4$ V (high overpotential), but similar nanostructures have been found at other applied potentials. Platinum, though, forms irregular porous dendritic nanostructures rather than hemispherical nanoparticles, as indicated by the growth pathways *'c'* and *'d'*. Although lattice fringes extend through large domains within the nanostructures, domains with different crystallographic orientation, spherical protuberances, coalescence necks, stacking faults, and twinning planes prove that the main growth mechanism is based on the aggregation, self-alignment, and partial coalescence of nanoclusters of $d \approx 2$ nm.[38] Growth pathways *'c'*and *'d'* represent the electrodeposition of platinum at $E \leq -0.4$ V and $E \geq -0.4$ V, respectively. These two regimes will be considered hereafter as high and low overpotentials, respectively, for the sake of clarity. Low overpotentials lead to open ultraporous nanodendrites due to limited coalescence, whereas high overpotentials result in less porous structures with smoother features, due to a higher degree of recrystallization and direct addition of Pt atoms.

A first important conclusion derived from this analysis is that the Electrochemical Aggregative Growth Mechanism is common for two metals from different rows and columns from the periodic table such as Ag and Pt. Therefore, it can be suggested as a general metal electrodeposition mechanism onto low energy substrates such as carbon. Second, recrystallization and coalescence kinetics are dependent on material, overpotential, and adsorbed species, and dictate the morphology of the final nanostructures to a large extent. Third, direct incorporation of Ag and Pt atoms can obviously not be excluded from the growth process. The analysis of the morphologies and crystallographic structures shown in Figure 1 indicates that such a growth mechanism is only noticeable after the aggregates have undergone a high degree of recrystallization. However, the direct attachment of reduced metal ions on individual nanoclusters or aggregates may as well influence recrystallization processes by acting as cohesive forces between adjacent nanoclusters or aggregates. To fully understand the described mechanism and its different growth pathways, an evaluation of electrochemical chronoamperograms and resulting nanoparticle size distributions is carried out in the next sections. Such analyses have been carried out on countless occasions to study electrochemical nucleation and growth processes, assuming that growth occurs by direct attachment. However, to perform these analyses in terms of our proposed mechanism, some additional concepts need to be taken into account. These concepts are nanocluster self-limiting growth, nanocluster surface diffusion, and nanocluster coalescence and recrystallization. Although frequently used in other new phase formation fields, these concepts are not often used in electrochemical deposition studies, and so they are described in general terms in the next section. Besides, explanations are provided on how they may be affected by the different processes occurring during electrochemical deposition.

Notes on Nanocluster Self-Limiting Growth, Electrochemical Potential Driven Surface Diffusion and Coalescence. *Self-Limiting Growth.* The self-limiting growth concept is probably the most difficult to understand, because although it has been reported in other fields, little is known about it. It has been sometimes attributed to closed-shell magic sizes.[15,21,40] Such full-shell configurations can be thought of as metastable states which constitute a local minimum of the function relating the change in free Gibbs energy of a growing particle with its radius, $\Delta G(r)$, which would otherwise decrease monotonically for radii larger than the critical radius. The reason for this to happen would be linked to a higher stability of certain facets, as opposed to the models which consider unfaceted hemispherical islands with an average surface energy.

In other cases, nanocluster self-limiting growth mechanisms are explained by particle stabilization due to adsorption of different species.[41] In an electrochemical deposition system, the latter would mean that some of the electrolyte species would be specifically adsorbed on the nanoclusters. blocking epitaxial growth on their surface.

Nanocluster Surface Diffusion. Nanocluster surface diffusion is never considered in electrochemical deposition systems because one of the key assumptions common to every model is that single adatoms are the only diffusing species over the substrate. In this way, nuclei are always considered as fixed islands pinned to specific sites on the surface. However, provided that it is widely accepted that adatoms can perform

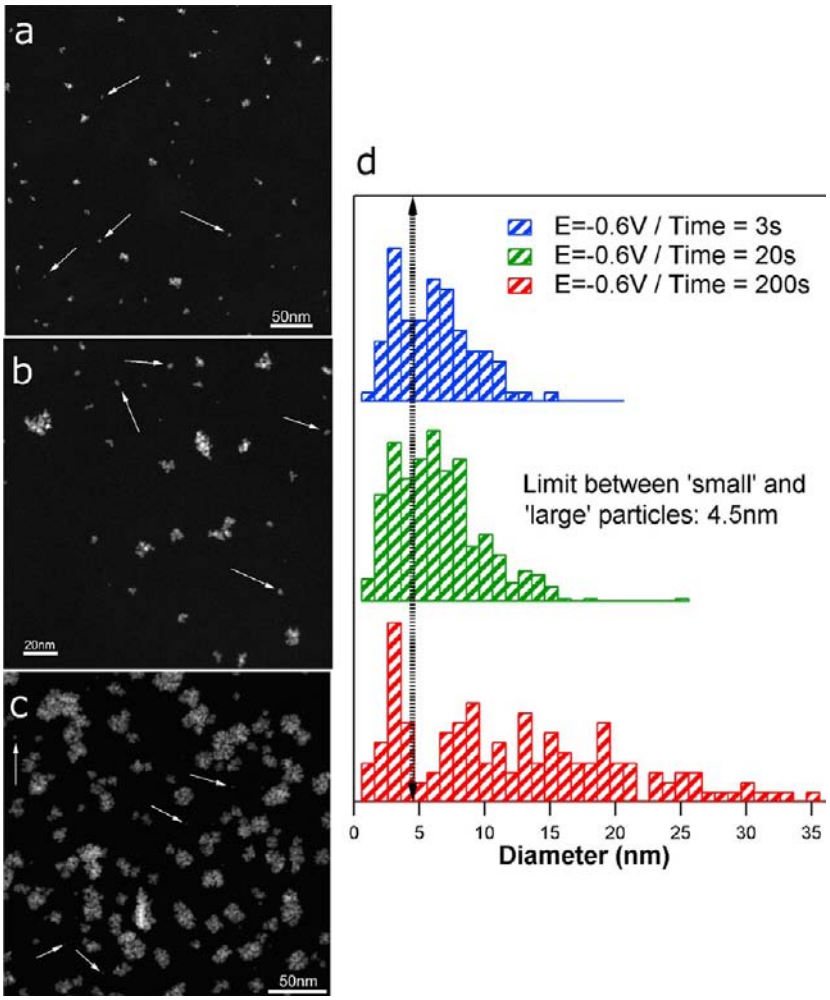

Figure 2. Representative low magnification HAADF-STEM pictures after the electrodeposition of platinum onto CCTGs at a potential of −0.6 V for (a) 3, (b) 20, and (c) 200 s. (d) Corresponding size histograms showing a bimodal size distribution.

random walks until they coalesce forming a stable nuclei,[12,13,39] it seems perfectly logical to assume that nanoclusters could experience the same phenomena, provided they are small enough. Indeed, temperature activated or accelerated nanocluster surface diffusion has been thoroughly studied.[42−45]

At high temperatures, it is proven that nanoclusters can perform a random walk over a surface similar to what atoms do, because nanoclusters of a few nm have surface diffusion coefficients of the same magnitude than those of single atoms.[43,46] However, it is also reported that, at room temperature (RT), nanocluster surface diffusion coefficients over glassy carbon are considerably smaller.[43,47] In our case, Ag and Pt nanoclusters have been imaged by HAADF-STEM and proven stable at RT, even under exposure to the electron beam.[33,38] Accordingly, it can be inferred that Ag and Pt nanoclusters do not diffuse at RT conditions under air or vacuum environments. Hence, cluster diffusion should occur during electrodeposition. We have also observed that nanocluster surface diffusion under open circuit potential is negligible. Hence, cluster movement in electrochemical deposition systems must be driven by the application of an electrochemical potential. Under electrochemical polarization, one could think of interparticle electrostatic interactions, but even if they were attractive, they would be screened by the supporting electrolyte within a few nm of their surface, ruling out long-range interparticle attractions.[48] Also, VDW interparticle attractive interactions, which are responsible for aggregation, cannot drive nanocluster surface diffusion over long distances because their range extends only for a few nm.

To find a plausible explanation, one has to look in more detail at the mechanisms by which nanocluster surface diffusion takes place. Provided they are small enough, it is commonly accepted that nanoclusters move randomly over surfaces by atom evaporation/recondensation processes leading to displacement of their center of mass, or by stress related dislocations between their crystallographic planes.[43,44,49] In this context, the cluster diffusion coefficient is proportional to the adatom density on the cluster surface and inversely proportional to r^4. When a material is heated to temperatures close to its melting point, more and more atoms get enough vibrational energy to instantaneously overcome the energy which binds them to the lattice. Therefore, the concentration of free adatoms on the cluster surface increases and so does the cluster surface diffusion coefficient, explaining temperature activated cluster diffusion. On the other hand, inherent to any electrochemical deposition system, metallic nanoclusters are in equilibrium with an aqueous phase with ions of the same metal. Therefore, when a negative potential is applied, metal ions are reduced all over the active surface. Therefore, the adatom density on the cluster surface increases, and so do nanocluster

dx.doi.org/10.1021/ja402598k | J. Am. Chem. Soc. 2013, 135, 11550−11561

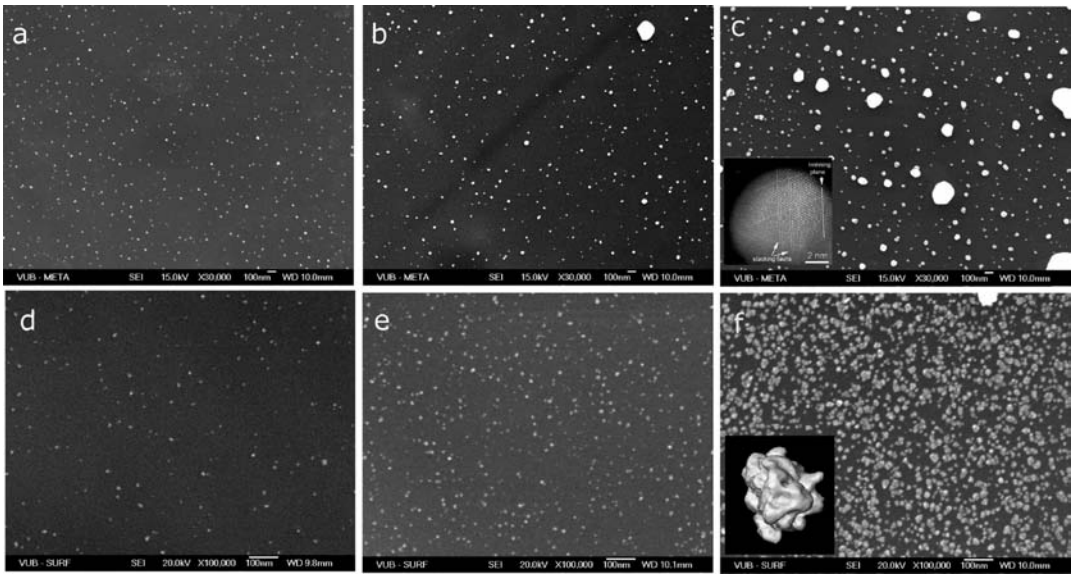

Figure 3. Representative FESEM pictures after the electrodeposition of silver onto CCTGs at a potential of −0.4 V for (a) 10, (b) 100, and (c) 500 ms. Representative FESEM pictures after the electrodeposition of platinum onto CCTGs at a potential of −0.6 V for (d) 3, (e) 20, and (f) 200 s. Insets: high magnification HAADF-STEM figure of a monocrystalline silver nanoparticle (c) and 3D reconstruction of a porous platinum nanostructure (f).

surface diffusion coefficients, without the need to apply higher temperatures. In some cases, electrochemical potential driven nanocluster surface diffusion has been detected under large anodic polarization in electrolytes not containing the corresponding metal ions.[49,50] We believe that such movement is also based on an increase of metal free adatoms on the surface of the nanoclusters. The difference would be that this time such free atoms would have been stripped off the cluster rather than discharged from the electrolyte. Therefore, in an electrochemical deposition system, the higher the overpotential is, the higher the nanocluster surface diffusion coefficients should be. This is difficult to assess experimentally, because reaction kinetics, nucleation rate, and particle coalescence also depend on the overpotential, being very difficult to distinguish its effect on cluster surface diffusion.

Nanocluster Coalescence. Nanocluster coalescence has normally been studied by using temperature or the incidence of highly energetic beams as sources of energy.[51,52] In these cases, when temperatures close to the melting point are reached, surface atoms get a high vibrational energy and can escape the crystal lattice increasing the concentration of free metal adatoms on the nanoparticle surface. It is proven that the mobility of these adatoms drives the coalescence process, and consequently, materials with low melting point experience faster recrystallization at lower temperatures. Accordingly, the aggregation of low melting point metal nanoclusters in colloidal synthesis leads to silver,[21,22] bismuth,[24] or gold spherical nanoparticles,[20,23] whereas high melting point metals such as platinum or palladium lead to porous nanodendrites.[27,29]

Along with the aforementioned theory for nanocluster surface diffusion, the application of high overpotentials would induce a large adatom density on the nanocluster surface, inducing faster recrystallization kinetics. This could explain that nanocluster coalescence processes under electrochemical polarization are accelerated with increasing overpotential[38] and are much faster for silver than for platinum.[33] In addition, the complex surface structures generated under electrochemical polarization may have an influence on coalescence kinetics as well. Therefore, it is logical to believe that specific adsorption of some chemical species could hinder the recrystallization process whereas others could catalyze it. Therefore, achieving the right balance between these interactions seems essential to build up nanostructures from nanocluster aggregation in an appropriate way.

Evaluation of Nanoparticle Size Distributions. Traditionally, FESEM or AFM/STM have been used for this purpose. However, FESEM analysis has been shown to fail when nanoparticles of $d \leq 5$ need to be resolved.[37] Besides, measurements of particle sizes by AFM/STM have been shown to be greatly affected and altered by the geometry of the tip,[53] and can induce cluster detachment and movement on its own.[54] Alternatively, the use of carbon coated TEM grids as electrochemical electrodes allows a proper evaluation of nanoparticle number, size, and spatial distribution over the whole size range by performing HAADF-STEM observations at low magnification. By means of this approach, we have recently shown that the early stages of silver electrodeposition lead to bimodal size distributions, where 'large' particles grow in size with increasing deposition time but small nanoclusters of $d \approx 1-2$ nm do not grow and eventually disappear, consumed by incorporation into larger aggregates.[33] These phenomena are commonly related to nanoparticle self-limiting growth and aggregation.[17,23,24]

In the case of platinum, similar phenomena occur and bimodal size distributions are also established during the early stages of electrodeposition at high overpotentials, as shown in Figure 2. However, almost no isolated platinum primary nanoclusters are found when smaller overpotentials are applied. This indicates that at low overpotentials cluster diffusion/aggregation predominates over nucleation, and vice versa. Therefore, although both rates are faster at high overpotentials, the nucleation rate is more strongly affected than the cluster diffusion/aggregation rate. Understanding such processes is extremely important, as the outcome of the electrodeposited nanostructures depends strongly on the balance betweeen

dx.doi.org/10.1021/ja402598k | J. Am. Chem. Soc. 2013, 135, 11550−11561

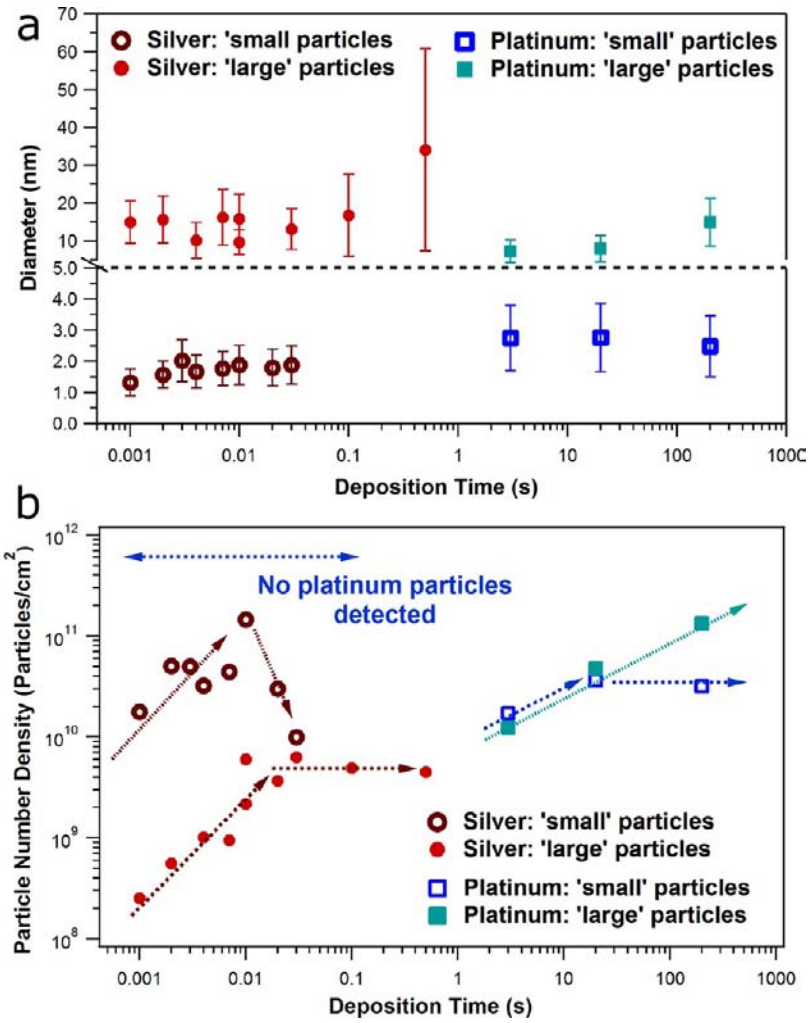

Figure 4. Time evolution of silver and platinum nanoparticle (a) average diameter and (b) number density after electrodeposition onto CCTGs at potentials of −0.4 and −0.6 V, respectively.

nucleation and nanocluster surface diffusion, which are both overpotential dependent.

HAADF-STEM images such as these from Figure 2 are used to elaborate statistics of the small particle populations, whereas FESEM pictures are used for the large particle populations. Figure 3 shows characteristic FESEM pictures presenting an overview of the distribution of silver (a–c) and platinum (d–f) nanoparticles electrodeposited at high overpotentials and different deposition times. The insets in (c) and (f) show a high resolution picture and a three-dimensional reconstruction of representative nanostructures obtained by aberration-corrected HAADF-STEM and electron tomography, respectively.[33,38] Figure 4 shows the corresponding evolution of average diameter (a) and particle number density (b) of both 'large' and 'small' particle populations for silver and platinum electrodeposition. Silver nanoparticles are formed at much shorter deposition times than platinum due to differences in reaction kinetics and so the deposition time is represented in logarithmic scale for the sake of comparability.

Figure 4a shows that small particles do not grow with deposition time in any of the cases. However, the size of such isolated small clusters is material dependent as Ag small nanoclusters have $d \approx 1.8 \pm 0.6$ nm (relative size dispersion ≈33%), whereas Pt small nanoparticles have a larger diameter of $d \approx 2.9 \pm 0.9$ nm (relative size dispersion ≈31%). This implies that a self-limiting growth mechanism prevents the growth of primary nanoclusters and stabilizes particles of different sizes depending on the material. On the other hand, we have shown that Pt aggregates which undergo a very small amount of recrystallization still show a self-limiting growth mechanism, whereas fully recrystallized aggregates do not.[38] One possible explanation, linked to closed-shell magic sizes, would be that the nanoclusters have a metastable atomic configuration, which hinders epitaxial growth, but become unstable after coalescence. However, in all the cases, primary nanoclusters have a relatively large size dispersion (33%), indicating that adsorption-driven stabilization is more plausible than closed-shell magic sizes. Therefore, another possible explanation would be that stabilization is related to specific adsorption onto the exposed facets of the primary nanoclusters, which change after coalescence. On the other hand, Figure 4a also shows that 'large' Ag and Pt nanoparticles only start to grow after a certain induction time ($t_{Ind} \approx 30$ ms for Ag; $t_{Ind} \approx 10$ s for Pt); before this time their size remains more or less constant ($d \approx 15 \pm 5$ nm for Ag; $d \approx 8 \pm 2$ for Pt). An induction period is a recurrent concept under many scenarios of new phase nucleation and growth, and it is normally ascribed to the time lapsed during nucleation and before the onset of particle growth.[15] In electrochemical deposition, induction periods are normally correlated to the establishment of an

dx.doi.org/10.1021/ja402598k | J. Am. Chem. Soc. 2013, 135, 11550–11561

electrochemical double layer and the discharge of metal atoms onto the electrode prior to nucleation.[13,31] However, we show that the induction time corresponds to the aggregation of primary nanoclusters onto larger entities which may grow at later stages.[33] Such a phenomenon, which can be considered an aggregate-nucleation process, has been recently reported in the field of colloidal synthesis.[23,24] In the case of Ag electrodeposition, such induction time corresponds to the period in which the number of aggregates increases by the assembly of isolated primary nanoclusters. Figure 4b shows that, after the induction period ($t_{Ind} \approx 30$ ms), no more aggregates are created because the surface has been depleted of primary nanoclusters. In the case of platinum, large aggregates start to grow after $t_{Ind} \approx 10$ s, but small primary clusters are continuously being formed on the carbon surface and, consequently, more and more large aggregates are also created continuously.

In fact, if one looks at the evolution of the aggregate diameter (a) and number density (b) with the surface coverage, shown in Figure 5, it becomes clear that in the case of silver, the number of aggregates reaches saturation at small surface coverages of about 1%, whereas for platinum, the large particle number density keeps increasing even at large surface coverages of about 30−40%. Correspondingly, for silver, the large particle size starts to increase at low surface coverage, whereas platinum aggregates remain small even after large surface coverage has been reached. Under the assumption of growth by direct attachment, growth under diffusion control generates diffusion zones around growing islands of about 10 times their diameter.[55] This would imply that when diffusion fields cover the whole surface, surface coverage should be about 1%. This is exactly the case for silver electrodeposition, indicating that silver aggregates grow by direct attachment under diffusion control. This behavior is confirmed by their monocrystalline structure after long deposition times, shown in the growth pathway *'a'* of Figure 1. Such generation of diffusion zones around the growing aggregates implies that the concentration of ions close to the surface gets gradually smaller, which in turn implies that, after a certain moment, no more primary clusters and hence no more aggregates can be generated. On the other hand, Figure 5b shows that the number of platinum aggregates keeps increasing at high surface coverages meaning that new primary nanoclusters are continuously generated over the carbon surface. This implies that no diffusion fields (or very small) are created around the aggregates, which in turn indicates that their growth by atomic incorporation is not limited by diffusion of active species toward the surface. This would be logical in the case that platinum deposition occurred under kinetic limitations, but this is not the case. When the applied potential is $E = -0.6$ V, the applied overpotential is large enough to rule out kinetic control (see Supporting Information, Figure S1). Therefore, it can be asserted that platinum aggregates do not grow by direct attachment to a large extent.

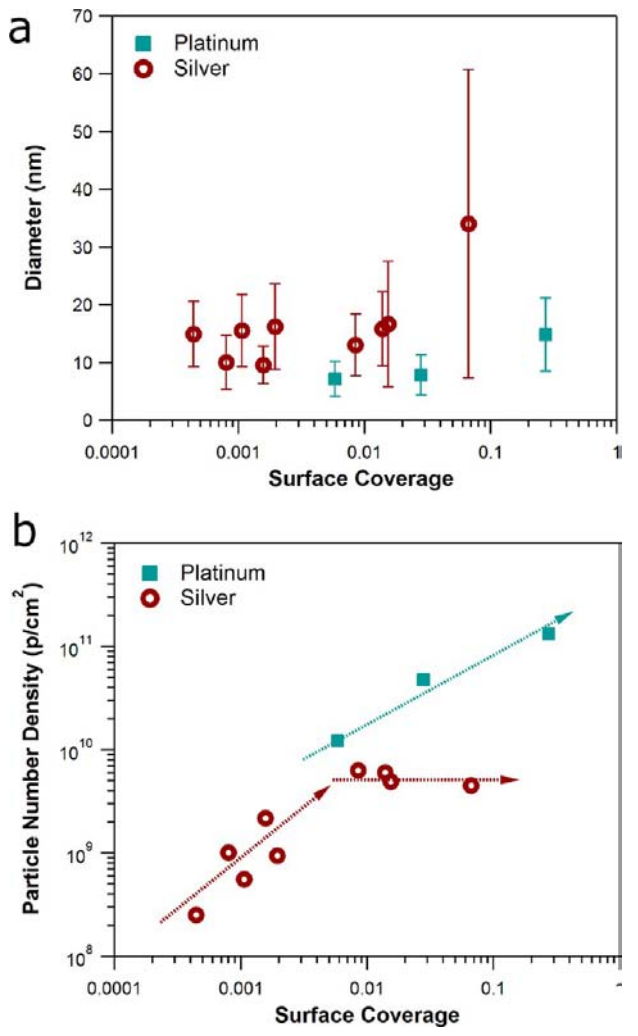

Figure 5. Evolution of 'large' particle (a) average diameter and (b) number density with surface coverage for silver and platinum electrodeposition onto CCTGs at potentials of −0.4 and −0.6 V, respectively.

As shown in Figure 1, the main difference between platinum and silver growth pathways is the fact that silver aggregates recrystallize into monocrystalline nanoparticles whereas platinum forms porous dendritic structures which only seem to partially recrystallize at large overpotentials. Therefore, silver aggregates behave as traditional islands and grow by atomic incorporation once they have undergone total recrystallization. This is why the evaluation of large particle or aggregate distributions follows the trends established by conventional electrochemical nucleation and growth theories and correlates with classical chronoamperommetric models with good agreement.[33] On the other hand, partially recrystallized platinum dendritic nanostructures behave halfway between growing islands and small 'stabilized' nanoclusters which cannot grow due to a self-limiting growth mechanism. Therefore, even under electrochemical diffusion control conditions, the evaluation of particle morphology and size distribution does not follow the assumptions of the Volmer−Weber 3D island growth mechanism.

Evaluation of Chronoamperommetric Data. Electrochemical deposition processes can be followed in situ by recording the current (or potential) transients during the application of different potential (or current) pulses. In the case of potentiostatic single pulse electrodeposition, the evaluation of the current−time transients, or chronoamperograms, provides invaluable time-resolved information about nucleation and growth processes and it is hence performed in countless occasions.[30,31] However, the analysis has been proven ineffective to explain experimental observations in many cases.[31−33]

Figure 6 shows the potentiostatic current transients obtained for silver (a) and platinum (b) electrodeposition. The analysis

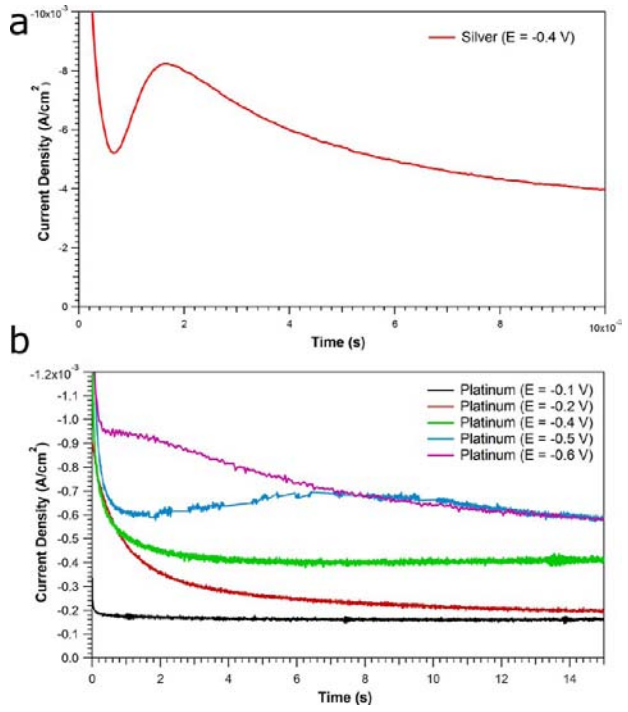

Figure 6. Chronoamperommetric current transients obtained for the electrodeposition of (a) silver and (b) platinum onto CCTGs.

of the silver current transients according to the classical electrochemical island growth models has been carried out in our previous work.[33] The calculated nucleation rate, AN_0, is in agreement with the number of 'large' aggregates derived from HAADF-STEM analysis, which follows an exponential trend according to $N_{\text{Aggregates}}(t) = N_0[1 - \exp(-At)]$. Silver aggregates, which have fully recrystallized into monocrystalline islands, grow by direct attachment. Hence, the assumptions from the classical models are fulfilled and good agreement between experimental and theoretical data is achieved. Yet, the analysis of the initial current decay is not straightforward. Traditionally, initial high current and fast decays have been associated to double layer charging.[56] However, double layer capacitive currents are expected to have an effect in the first microseconds, so the extension of this phenomenon to the millisecond time frame is uncertain. Therefore, the current consumed during long-term decays must be of faradaic origin. More appropriately, it has been postulated that such decays may be a consequence of 2-dimensional surface reaction phenomena, such as metal adatom adsorption[32] or formation of subcritical nuclei on the bare electrode surface.[57] Monotonically decaying currents are also typical from underpotential deposition[58] or layer-by-layer growth, where 3-dimensional growth does not occur. We believe that the initial current decay is caused by the formation of primary nongrowing nanoclusters instead. Traditional island growth is characterized by an increasing current due to the hemispherical diffusion to growing centers, which in turn leads to an increase in the active surface area.[13,30] However, we have shown that primary clusters do not grow by atomic addition beyond a few nm, so they do not contribute substantially to an increase of the active area, and the faradaic current consumed by the formation of these clusters will have planar diffusion Cotrellian characteristics ($I \propto t^{-(1/2)}$) of monotonic decaying nature.

In fact, the current−time transients obtained for the early stages of platinum electrodeposition do not display the typical peaked shape characteristic of the 3D island growth mechanism.[13,30] At $E = -0.1$ V, $I(t)$ has a constant value, characteristic of a charge-transfer limited electrochemical reaction. However, it must be pointed out that kinetically limited island growth should lead to an increasing current density due to an increasing active surface area, until physical island overlap is reached. This is not the case, indicating that the deposited islands do not act as active surface area for direct atomic incorporation. Under these conditions, platinum aggregates are ultraporous nanostructures which have not undergone any recrystallization, and present no signs of growth by direct attachment (Figure 1, growth pathway '*d*'). At $E = -0.2$ V, $I(t)$ shows long-term decay characteristics that cannot be due to double-layer charging because they extend over ≈15 s. The current decay in this case is due to the fact that platinum reduction takes place in diffusion-limited or mixed-control regime (see Supporting Information, Figure S1). Still, no signs of current increase indicate that primary nanoclusters are being formed under planar diffusion limitations and that large aggregates are not contributing to an increase in active surface area for direct attachment. This is again correlated to the ultraporous nanodendritic morphology obtained at these potentials (Figure 1, growth pathway '*d*'). At $E = -0.4$ V, $I(t)$ starts by a long-term decay, followed by a slight increase in current indicating that a certain degree of uncoupled diffusion toward growing active centers occurs. At $E = -0.5$ V and $E = -0.6$ V, current starts increasing at earlier times indicating an earlier onset of island growth by direct attachment. This is again linked with the fact that the obtained nanostructures have undergone a certain degree of recrystallization and are thus smoother and less porous than those obtained at smaller overpotentials (Figure 1, growth pathway '*c*'). Both curves show a current maximum which is normally correlated to the overlap of the diffusion zones.[30,31] However, experimental FESEM and HAADF-STEM observations have shown that the carbon surface is always accessible for the formation of new primary nanoclusters. Therefore, a total overlap of the diffusion zones cannot be occurring, as this would lead to a halt of primary cluster nucleation and consequent saturation of aggregate number density. Alternatively, partial coalescence of some diffusion fields or physical coalescence upon growing islands could explain a current maximum and would not imply complete inhibition of nucleation on the carbon surface. Instead, this would lead to a gradual decrease of the nucleation rate, which is observed experimentally, as shown in Figures 4b and 5b.

It must be noted that platinum electrodeposition occurs together with different hydrogen reduction reactions catalyzed by the actual platinum surface (see Supporting Information, Figure S1). Therefore, the obtained current−time transients represent a convolution of both phenomena. However, recent studies show that the effect of the hydrogen reduction component on the current transient is only remarkable at long deposition times, by deviating the transient from the typical Cotrellian behavior ($I \propto t^{-(1/2)}$). Hence, it should not substantially change its characteristic peaked shape at the beginning of the transient,[59] so it does not influence our interpretation of the current transients. It must be noted as well that several reports on platinum electrodeposition on carbon substrates have shown peak-shaped current transients modeled by means of classical electrochemical island growth mecha-

dx.doi.org/10.1021/ja402598k | J. Am. Chem. Soc. 2013, 135, 11550−11561

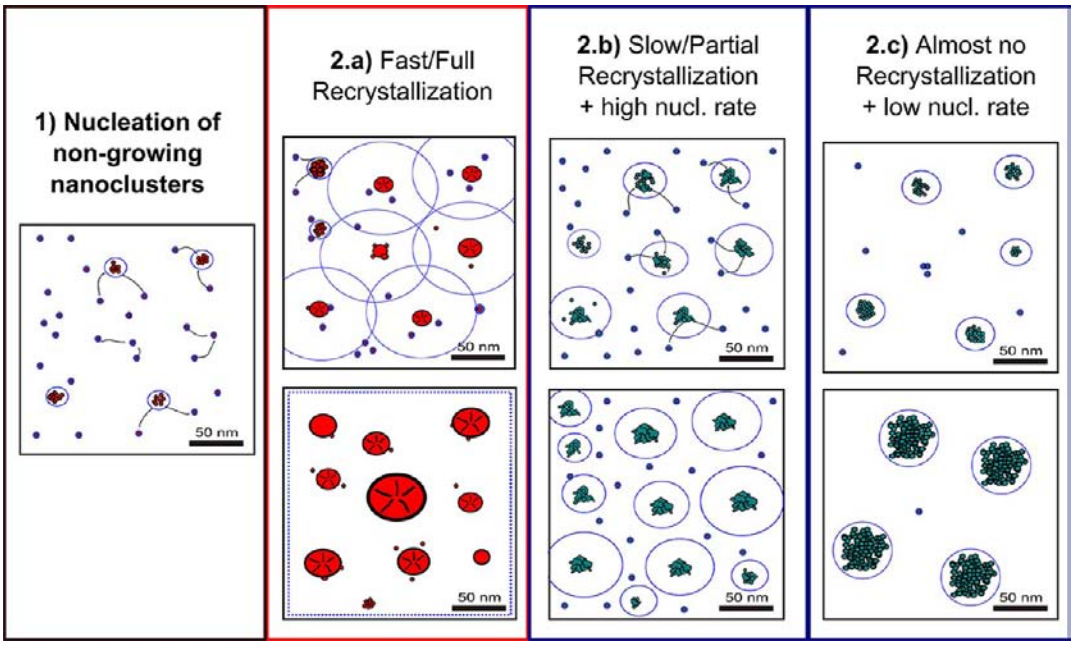

Figure 7. Schematic diagram showing the different stages of the Generalized Electrochemical Aggregative Growth Mechanism. Dots represent the nongrowing nanoclusters and blue circles around the aggregates represent the projection of their corresponding nucleation exclusion zones. Black stripes within a particle represent defects whereas the absence of stripes represents a defect-free monocrystalline structure.

nisms. However, in most of the cases, even if current transients can be fitted to classical models, the difference in number density between experimental and calculated values may rise up to several orders of magnitude,[35] as it happens with other metals.[32,59] As an example, the current transient obtained at $E = -0.5$ V can be fit to the instantaneous nucleation equation[30] leading to a saturation particle density of $N = 4 \times 10^5$ particles/cm^2, 5 orders of magnitude smaller than the value of 3×10^{10} observed experimentally[38] (see Supporting Information Figure S3). Therefore, according to classical island growth models, the charge of such a potentiostatic experiment would have been consumed to grow ≈10 000 times less particles that would have had a diameter ≈46 times larger. The fact that we experimentally observe many more particles and much smaller than predicted by the models points again to a self-limiting growth mechanism, which prevents primary nanoclusters to grow by atomic incorporation.

Revision of the Nucleation and Growth Mechanism: Generalized Electrochemical Aggregative Growth Mechanism. In conclusion, the data presented throughout this paper together with the findings of our previous work[33,38] indicate that metal electrodeposition onto low energy substrates such as carbon proceeds by a Generalized Electrochemical Aggregative Growth Mechanism instead of by a classical Volmer–Weber mechanism. The proposed mechanism starts with the nucleation of primary nanoclusters that grow until a certain self-limiting growth mechanism stabilizes them at a given size. Then, electrochemical potential driven surface diffusion of these primary nanoclusters leads to aggregation, which can be interpreted as aggregative-nucleation events. Finally, the degree to which aggregates undergo partial or full coalescence dictates to which extent further growth by direct attachment (or classical island growth) occurs. Figure 7 schematically represents the stages of the proposed mechanism. Its implications on the interpretation of the potentiostatic current transients, nanoparticle morphology, number, and size distribution are shown in Figures 8, 9, and 10.

In the first moments after the application of a negative potential, very small primary nanoclusters are formed, randomly distributed over the substrate as shown by Figure 7.1. These clusters are single crystalline nanoparticles that grow by direct attachment until they reach a metastable size, with $d \approx 1.8 \pm 0.6$ nm for Ag and $d \approx 2.9 \pm 0.9$ nm for Pt. These size-stabilized primary nanoclusters can diffuse over the carbon surface due to their small size and weak van der Waals (VDW) forces between them and the carbon support. Due to particle–particle attractive VDW forces, primary nanoclusters stick together when they hit each other resulting in aggregative-nucleation events, which give birth to aggregated particles from nanocluster building blocks (Figure 7.2 and second column of Figure 1). Silver aggregates (Figures 7.2a and 1b) are much more compact than platinum ones (Figures 7.2b, 7.2c, 1c, and 1.d) because they undergo more and faster recrystallization. Until this stage, new primary nanoclusters and consequently new aggregates are continuously formed on the substrate in both cases, because even under the assumptions of island growth by direct attachment, the diffusion zones of potentially growing nuclei would not yet have covered the whole carbon surface.

An important point here is related to the interpretation of the electrochemical current–time transients. Traditionally, the first decaying part is related to double layer charging, whereas island nucleation and growth is correlated to hemispherical diffusion to an increasing active surface, leading to an increasing current. We have shown though that longer current decays should be of faradaic origin, and hence we believe that such $I(t)$ feature reflects the formation of primary nanoclusters which do not grow beyond a given size. This period may be considered an induction time because large aggregates do not yet grow significantly. Such a phenomenon is normally correlated to a prenucleation stage where metal ions are being discharged

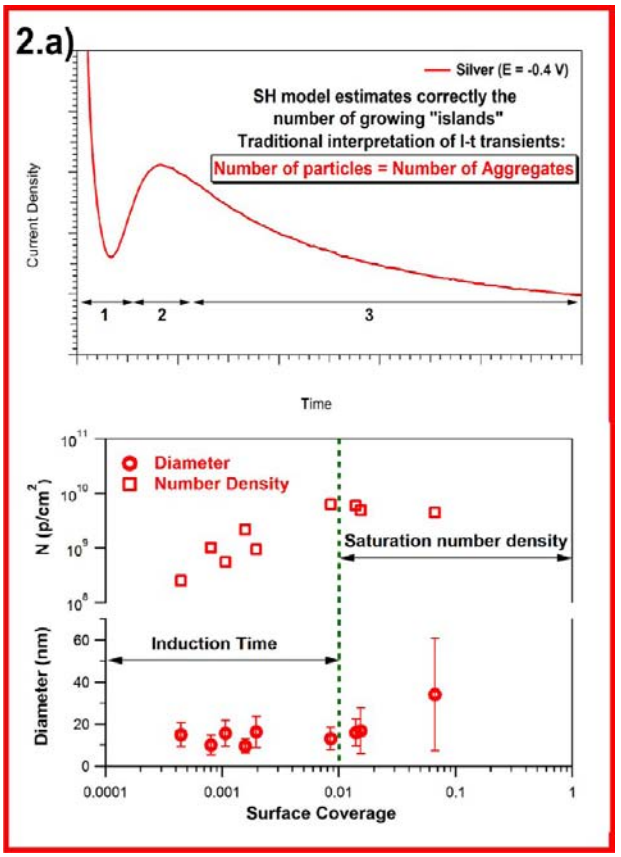

Figure 8. Full recrystallization. (1) Induction time: Formation of nongrowing primary nanoclusters, (2) Formation of primary nanoclusters + uncoupled "island" growth of completely recrystallized aggregates, (3) Coupled "island" growth of completely recrystallized aggregates.

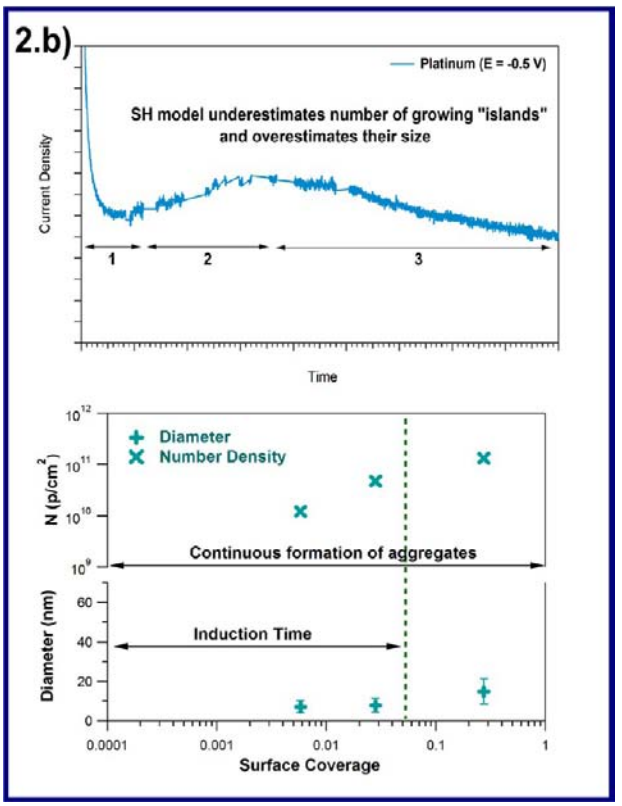

Figure 9. Partial recrystallization. (1) Induction time: Formation of nongrowing primary nanoclusters, (2) Formation of primary nanoclusters + uncoupled "island" growth of partially recrystallized aggregates, (3) Formation of primary nanoclusters + coupled "island" growth of partially recrystallized aggregates.

before nuclei have been formed. However, we believe that such induction time corresponds to a preaggregation or precoalescence stage where primary nanoclusters have already nucleated but cannot grow over a given size unless they undergo aggregation and recrystallization. Subsequent current rise and maximum are due to the growth of recrystallized aggregates (see Figures 8, 9, and 10). In fact, the degree to which such aggregates undergo recrystallization and coalescence dictates the subsequent growth pathways that lead to different particle morphologies. This has not been reported previously for electrochemical deposition systems, but similar phenomena can be found in other thin-film growth methods, such as deposition of mass selected preformed clusters.[45]

A first possibility is that the aggregates fully coalesce and recrystallize fast into monocrystalline nanoparticles (Figures 7.2a and 1b), as happens for silver electrodeposition. Then, the self-limiting growth mechanism vanishes and the particles may grow by direct attachment. Proof is given by the fact that silver nanoparticles after long deposition times are always monocrystalline.[33] This is probably the most common case and it implies that classical island growth concepts apply. Thus, diffusion zones are generated around growing particles until they cover the entire surface and particle number density reaches saturation at small surface coverages of 1%, while small primary nanoclusters are consumed. Therefore a classical interpretation of the potentiostatic current−time transients can be carried out taking into account that the derived nucleation rate corresponds to an 'aggregative-nucleation + recrystallization' rate rather than to primary nanocluster formation[33] (see Figures 8 and 6a).

A second possibility is that aggregates undergo partial recrystallization, as happens for platinum electrodeposition at high overpotentials (Figures 7.2b and 1c). In this case, classical growth concepts do not apply, as partially recrystallized aggregates behave halfway between traditional islands and nongrowing clusters. This way, small diffusion zones may be generated around growing aggregates, slowing down the nucleation rate of both primary nanoclusters and aggregates. However, the extent to which the particles grow by direct attachment is smaller than in the first case, and hence, diffusion zones do not cover the entire surface until longer deposition times. In this case, particle number density keeps increasing even at high surface coverages. The fact that many aggregates do not grow by atomic incorporation may favor the nucleation of new primary nanoclusters, as discharged atoms may be repelled by nongrowing particles, thus increasing their concentration on the carbon surface. In this case, the shape of the current transients depends on the degree of coalescence, recrystallization, and growth by direct attachment. High recrystallization rates imply a higher amount of ions directly reduced on growing aggregates, which in turn leads to a first increase in reactive surface area and a later development and coalescence of diffusion fields. In these cases, peaked $I(t)$ profiles are obtained after longer or shorter induction times in which the current monotonically decreases (Figures 9 and 6 for $E = -0.4$, -0.5, and -0.6 V). Such a peaked shape can be

dx.doi.org/10.1021/ja402598k | J. Am. Chem. Soc. 2013, 135, 11550−11561

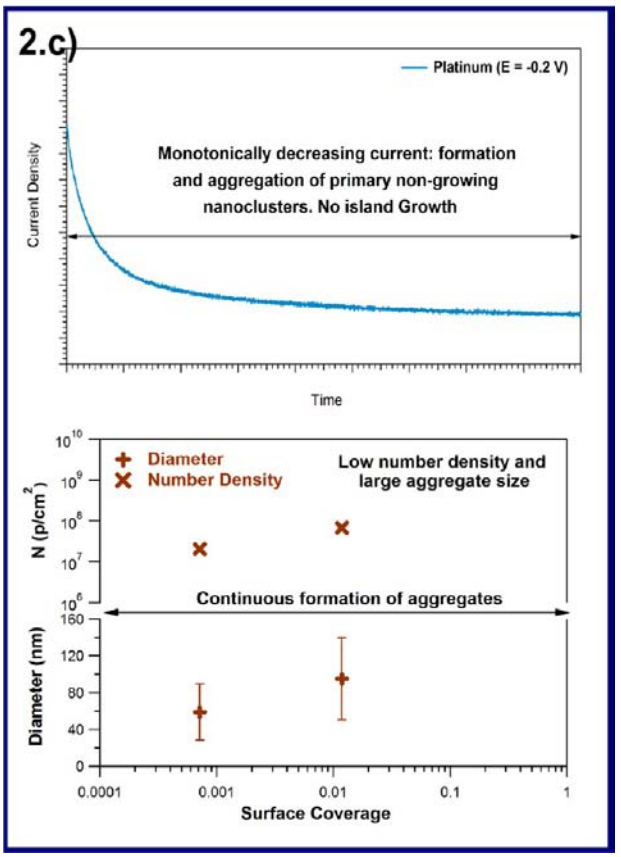

Figure 10. Almost no recrystallization. Continuous formation and aggregation of nongrowing primary nanoclusters.

correlated to an 'aggregative-nucleation + recrystallization' process from primary nanoclusters as building units.

A third possibility is that recrystallization happens to a very small extent leading to a lower degree of direct attachment (Figures 7.2c and 1d). In these cases, highly porous dendritic nanostructures are obtained, ever-decaying current transients are measured (Figures 10 and 6 for $E = -0.2$ V), and aggregates behave as nongrowing primary nanoclusters, which do not contribute to an increase in reactive surface area.

In conclusion, the Generalized Electrochemical Aggregative Growth Mechanism that we propose states that the early stages of electrochemical nucleation and growth are driven by primary nanocluster nucleation, self-limiting growth, surface diffusion, and aggregation. Then, later growth stages are driven by the extent of nanocluster coalescence, recrystallization, and growth by atomic incorporation. The balance between these phenomena dictates the resulting particle number density, size, and morphology, as well as the shape of the potentiostatic current transients and their interpretation.

CONCLUSIONS

By the combination of aberration-corrected HAADF-STEM, FESEM, and electrochemical characterization of different electrochemical deposition systems, we provide a complete reformulation of the Volmer–Weber island growth mechanism for the early stages of metal electrodeposition on low-energy substrates. We elaborate a Generalized Electrochemical Aggregative Growth Mechanism, which mimics the atomistic processes of the early stages of thin-film growth[39] by considering nanoclusters of a few nm as building blocks instead of single atoms. This way, we discuss the influence of new processes such as nanocluster self-limiting growth, surface diffusion, aggregation, and coalescence, on the growth mechanism, morphology of the resulting nanostructures, and interpretation of potentiostatic current transients. On one hand, self-limiting growth processes halt the growth of primary nanoclusters at a few nm, favoring a coalescence driven growth mechanism. The size of these clusters depends on the electrodeposited material but is independent of potential and deposition time. On the other hand, the morphology of the deposits depends strongly on the balance between nucleation and nanocluster surface diffusion, which are both overpotential dependent. In addition, nanocluster coalescence kinetics are proven to be material and overpotential dependent and of vital importance to determine further growth pathways. The degree to which nanoclusters are able to recrystallize drives nanoparticle morphology, size, number density, and surface coverage. Whereas a small extent of coalescence leads to ultraporous dendritic structures, large surface coverages, and small particle size; full recrystallization leads to larger hemispherical monocrystalline islands and smaller particle density. The latter case allows a traditional interpretation of the current transients taking into account that derived particle densities and nucleation rates reflect the formation and recrystallization of aggregates built up of primary nanoclusters rather than primary nuclei formation. In contrast, when coalescence occurs only to a small extent, aggregates behave halfway between traditional islands and nongrowing nanoclusters, so classical interpretation of the current-transients is not possible. Accordingly, the induction time, which can be extracted from particle distribution analyses and chronoamperommetric data, is related to aggregate-nucleation events rather than to standard nucleation processes. The model we propose, apart from being an important scientific breakthrough from the fundamental point of view, is crucial to gain better control of electrochemical deposition processes in order to obain supported nanostructures with desired morphology and enhanced properties. On top of that, understanding electrochemical potential driven nanocluster surface diffusion and coalescence is also crucial for the long-term stability of fuel cell catalysts, because one of their main failure mechanisms is the loss of catalytic surface area due to nanoparticle aggregation. Finally, achieving the right balance between nucleation, self-limiting growth, cluster surface diffusion, recrystallization, and coalescence kinetics is essential for the synthesis and operation of supported nanostructures, and it opens up new, exciting possibilities for electrochemical nanostructuring, with nanoclusters as building blocks.

ASSOCIATED CONTENT

Supporting Information

Cyclic voltammetry. Scharifker-Hills model fit for $E = -0.5$ V. This material is available free of charge via the Internet at http://pubs.acs.org/.

AUTHOR INFORMATION

Corresponding Author

*E-mail: hterryn@vub.ac.be.

Notes

The authors declare no competing financial interest.

■ ACKNOWLEDGMENTS

The authors acknowledge the support from the Fonds Wetenschappelijk Onderzoek in Vlaanderen (FWO, contract no. FWOAL527), the Flemish Hercules 3 programme for large infrastructure, and the Société Française de Bienfaisance et d'Enseignement (S.F.B.E.) de San Sebastian-Donostia (Spain). The authors would like to thank as well Dr. Patrick Steegstra and Luíca Fernández Macía for helpful discussions during the preparation of this manuscript.

■ REFERENCES

(1) Burda, C.; Chen, X.; Narayanan, R.; El-Sayed, M. a. *Chem. Rev.* **2005**, *105*, 1025−102.
(2) Chen, A. C.; Holt-Hindle, P. *Chem. Rev.* **2010**, *110*, 3767−3804.
(3) Yu, W.; Porosoff, M. D.; Chen, J. G. *Chem. Rev.* **2012**, *112*, 5780−817.
(4) Campbell, F. W.; Compton, R. G. *Anal. Bioanal. Chem.* **2010**, *396*, 241−259.
(5) Rassaei, L.; Marken, F.; Sillanpää, M.; Amiri, M.; Cirtiu, C. M.; Sillanpää, M. *TrAC, Trends Anal. Chem.* **2011**, *30*, 1704−1715.
(6) Xia, Y.; Xiong, Y.; Lim, B.; Skrabalak, S. E. *Angew. Chem., Int. Ed. Engl.* **2009**, *48*, 60−103.
(7) Mohanty, A.; Garg, N.; Jin, R. *Angew. Chem., Int. Ed. Engl.* **2010**, *49*, 4962−6.
(8) Lee, H.; Habas, S. E.; Kweskin, S.; Butcher, D.; Somorjai, G. a.; Yang, P. *Angew. Chem., Int. Ed. Engl.* **2006**, *45*, 7824−8.
(9) Tian, N.; Zhou, Z.-Y.; Sun, S.-G.; Ding, Y.; Wang, Z. L. *Science* **2007**, *316*, 732−5.
(10) Day, T. M.; Unwin, P. R.; Macpherson, J. V. *Nano Lett.* **2007**, *7*, 51−57.
(11) Becker, R.; Döring, W. *Ann. Phys.* **1935**, *416*, 719−752.
(12) Venables, J. A.; Spiller, G. D. T.; Hanbucken, M. *Rep. Prog. Phys.* **1984**, *47*, 399−459.
(13) Budevski, E.; Staikov, G.; Lorenz, W.; Keusler, K. *Electrochemical phase formation and growth*; Wiley-VCH, 1997.
(14) LaMer, V.; Dinegar, R. *J. Am. Chem. Soc.* **1950**, *72*, 4847−4854.
(15) Watzky, M. A.; Finke, R. G. *Chem. Mater.* **1997**, *9*, 3083−3095.
(16) Goris, B.; Bals, S.; Van den Broek, W.; Carbó-Argibay, E.; Gómez-Graña, S.; Liz-Marzán, L. M.; Van Tendeloo, G. *Nat. Mater.* **2012**, *11*, 930−5.
(17) Zheng, H. M.; Smith, R. K.; Jun, Y. W.; Kisielowski, C.; Dahmen, U.; Alivisatos, A. P. *Science* **2009**, *324*, 1309−1312.
(18) Murray, C. B. *Science* **2009**, *324*, 1276−7.
(19) Colliex, C. *Science* **2012**, *336*, 44−5.
(20) Polte, J.; Ahner, T. T.; Delissen, F.; Sokolov, S.; Emmerling, F.; Thünemann, A. F.; Kraehnert, R. *J. Am. Chem. Soc.* **2010**, *132*, 1296−301.
(21) Takesue, M.; Tomura, T.; Yamada, M. *J. Am. Chem. Soc.* **2011**, 14164−14167.
(22) Polte, J.; Tuaev, X.; Wuithschick, M.; Fischer, A.; Thuenemann, A. F.; Rademann, K.; Kraehnert, R.; Emmerling, F. *ACS Nano* **2012**, *6*, 5791−802.
(23) Shields, S. P.; Richards, V. N.; Buhro, W. E. *Chem. Mater.* **2010**, *22*, 3212−3225.
(24) Richards, V. N.; Shields, S. P.; Buhro, W. E. *Chem. Mater.* **2011**, *23*, 137−144.
(25) Niederberger, M.; Cölfen, H. *Phys. Chem. Chem. Phys.* **2006**, *8*, 3271−87.
(26) Ge, J.; Lei, J.; Zare, R. N. *Nat. Nanotechnol.* **2012**, *7*, 428−32.
(27) Lim, B.; Kobayashi, H.; Camargo, P. H. C.; Allard, L. F.; Liu, J.; Xia, Y. *Nano Res.* **2010**, *3*, 180−188.
(28) Finney, E. E.; Shields, S. P.; Buhro, W. E.; Finke, R. G. *Chem. Mater.* **2012**, *24*, 1718−1725.
(29) Mondloch, J. E.; Yan, X.; Finke, R. G. *J. Am. Chem. Soc.* **2009**, *131*, 6389−96.
(30) Scharifker, B.; Hills, G. *Electrochim. Acta* **1983**, *28*, 879−889.
(31) Hyde, M. E.; Compton, R. G. *J. Electroanal. Chem.* **2003**, *549*, 1−12.
(32) Radisic, A.; Vereecken, P. M.; Hannon, J. B.; Searson, P. C.; Ross, F. M. *Nano Lett.* **2006**, *6*, 238−242.
(33) Ustarroz, J.; Ke, X.; Hubin, A.; Bals, S.; Terryn, H. *J. Phys. Chem. C* **2012**, *116*, 2322−2329.
(34) Zoval, J. V.; Lee, J.; Gorer, S.; Penner, R. M. *J. Phys. Chem. B* **1998**, *102*, 1166−1175.
(35) Gloaguen, F.; Leger, J.; Lamy, C.; Marmann, A.; Stimming, U.; Vogel, R. *Electrochim. Acta* **1999**, *44*, 1805−1816.
(36) Plyasova, L.; Molina, I.; Gavrilov, A.; Cherepanova, S.; Cherstiouk, O.; Rudina, N.; Savinova, E.; Tsirlina, G. *Electrochim. Acta* **2006**, *51*, 4477−4488.
(37) Ustarroz, J.; Gupta, U.; Hubin, A.; Bals, S.; Terryn, H. *Electrochem. Commun.* **2010**, *12*, 1706−1709.
(38) Ustarroz, J.; Altantzis, T.; Hammons, J. A.; Hubin, A.; Bals, S.; Terryn, H. Manuscript submitted for publication , 2013
(39) Zhang, Z. Y.; Lagally, M. G. *Science* **1997**, *276*, 377−383.
(40) Tuinenga, C.; Jasinski, J.; Iwamoto, T.; Chikan, V. *ACS Nano* **2008**, *2*, 1411−1421.
(41) Besson, C.; Finney, E. E.; Finke, R. G. *J. Am. Chem. Soc.* **2005**, *127*, 8179−84.
(42) Thiel, P. A.; Shen, M.; Liu, D. J.; Evans, J. W. *J. Phys. Chem. C* **2009**, *113*, 5047−5067.
(43) Jensen, P. *Rev. Mod. Phys.* **1999**, *71*, 1695−1735.
(44) Jak, M.; Konstapel, C.; Kreuningen, A. V. *Surf. Sci.* **2000**, *457*, 295−310.
(45) Yoon, B.; Akulin, V.; Cahuzac, P.; Carlier, F.; de Frutos, M.; Masson, A.; Mory, C.; Colliex, C.; Bréchignac, C. *Surf. Sci.* **1999**, *443*, 76−88.
(46) Garbarino, S.; Pereira, A.; Hamel, C.; Irissou, E.; Chaker, M.; Guay, D. *J. Phys. Chem. C* **2010**, *114*, 2980−2988.
(47) Popescu, R.; Schneider, R.; Gerthsen, D.; Böttcher, A.; Löffler, D.; Weis, P.; Kappes, M. *Surf. Sci.* **2009**, *603*, 3119−3125.
(48) Cosgrove, T. *Colloid science: principles, methods and applications*, 2010
(49) Giesen, M. *Prog. Surf. Sci.* **2001**, *68*, 1−154.
(50) Hartl, K.; Nesselberger, M.; Mayrhofer, K. J. J.; Kunz, S.; Schweinberger, F. F.; Kwon, G.; Hanzlik, M.; Heiz, U.; Arenz, M. *Electrochim. Acta* **2010**, *56*, 810−816.
(51) José-Yacaman, M.; Gutierrez-Wing, C.; Miki, M.; Yang, D.-Q.; Piyakis, K. N.; Sacher, E. *J. Phys. Chem. B* **2005**, *109*, 9703−11.
(52) Asoro, M. A.; Kovar, D.; Shao-Horn, Y.; Allard, L. F.; Ferreira, P. J. *Nanotechnology* **2010**, *21*, 025701.
(53) Zoval, J. V.; Stiger, R. M.; Biernacki, P. R.; Penner, R. M. *J. Phys. Chem.* **1996**, *100*, 837−844.
(54) Tripathi, M.; Paolicelli, G.; D'Addato, S.; Valeri, S. *Nanotechnology* **2012**, *23*, 245706.
(55) Liu, H.; Penner, R. M. *J. Phys. Chem. B* **2000**, *104*, 9131−9139.
(56) Palomar-Pardave, M.; Miranda-Hernandez, M.; Gonzalez, I.; Batina, N. *Surf. Sci.* **1998**, *399*, 80−95.
(57) Gonnissen, D.; Simons, W.; Hubin, A. *J. Electroanal. Chem.* **1997**, *435*, 149−155.
(58) Mendoza-Huizar, L. H.; Robles, J.; Palomar-Pardave, M. *J. Electroanal. Chem.* **2002**, *521*, 95−106.
(59) Rezaei, M.; Tabaian, S. H.; Haghshenas, D. F. *Electrochim. Acta* **2013**, *87*, 381−387.